Dynamic Effects on the Mobilization of a Deposited Nanoparticle by a Moving Liquid-Liquid Interface

Tianya Yin, Donglee Shin, Joelle Frechette, Carlos E. Colosqui, and German Drazer

Phys. Rev. Lett. **121**, 238002 — Published 7 December 2018

DOI: 10.1103/PhysRevLett.121.238002

Dynamic effects on the mobilization of a deposited nanoparticle by a moving liquid-liquid interface

Tianya Yin[a], Donglee Shin[b], Joelle Frechette[b], Carlos Colosqui[c] and German Drazer[d]

[a] *Chemical Engineering Department, Rutgers, The State University of New Jersey, Piscataway, NJ.*

[b] *Chemical and Biomolecular Engineering Department, Johns Hopkins University, Baltimore, MD.*

[c] *Department of Mechanical Engineering, Stony Brook University, Stony Brook, NY.*

[d] *Mechanical and Aerospace Engineering Department, Rutgers, The State University of New Jersey, Piscataway, NJ.*

Abstract

Using molecular dynamics simulations, we investigate the fate of a nanoparticle deposited on a solid surface as a liquid-liquid interface moves past it, depending on the wetting of the solid by the two liquids and the magnitude of the driving force. Interfacial pinning is observed below a critical value of the driving force. Above the critical driving force for pinning and for large contact angle values we observe stick-slip motion, with intermittent interfacial pinning and particle sliding at the interface. At low contact angles we observe that particle rolling precedes detachment, which indicates the importance of dynamic effects not present in static models. The findings in this work indicate that particle mobilization and removal efficiencies originating in dynamic liquid-liquid interfaces can be significantly underestimated by static models.

The transport and fate of colloidal particles in porous media affects a broad range of phenomena, from the fouling of membranes used in water treatment and the effective permeability of oil and gas reservoirs, to the spreading of contaminants in the subsurface and possible remediation strategies [1–3]. Continuous progress has been made in our understanding and modeling since the introduction of *colloid filtration theory* in saturated systems [4], but predicting the mobilization and transport of nanoparticles remains challenging [5,6]. Unsaturated and multiphase flows in geological porous media present additional difficulties to predict nanoparticle transport, due to their dynamic interaction with moving interfaces between fluids phases [7]. A critical aspect that this works aims to understand is the remobilization of deposited colloidal particles by dynamic liquid-liquid interfaces and the moving (three-phase) contact line. This phenomenon plays a key role in various natural and industrial processes, such as groundwater transport in the vadose zone [8] and enhanced oil recovery operations [9]. Most of the available experimental work provides qualitative descriptions of the particle behavior, characterized by the average remobilization rate or removal efficiency. [10,11]. Only a small number of experimental studies have investigated the remobilization of individual particles by moving fluid interfaces in modeled porous media [12–14]. Moreover, these experimental studies were performed at a mesoscopic level (i.e., pore-level) and thus lack details of the physics at play for individual particles during remobilization events. It is necessary to investigate the different forces acting at the single-particle level to understand how dynamic processes affect colloidal detachment and remobilization [7]. In this work, we consider the motion of liquid-liquid interfaces past a single nanoparticle deposited on a flat wall and document the presence of different dynamic regimes, including interface pinning, stick-slip motion, and particle rolling and detachment, depending on the magnitude of the driving force and the contact angle that the interface forms with the particle. Moreover, we elucidate the dominant role of the surface tension forces acting on the studied nanoparticles and how such forces determine the emergence of different dynamic regimes. We also find that particle detachment cannot be accurately predicted by a static balance of surface tension and adhesion forces as it is in most cases preceded by particle rolling.

In previous work, using molecular dynamics (MD) simulations we showed that low-wettability liquids can induce the spontaneous adsorption of a nanoparticle to a solid wall [15–17]. In this work, we investigate the fate of a nanoparticle, initially deposited on a solid wall, as a three-phase contact line

moves past it, depending on the wettability of the two liquids. This problem has the essential components of the remobilization phenomenon encountered in multiphase-flows in porous media. The MD simulations were performed using the open-source package LAMMPS [18]. To model interactions between any pair of atoms *i* and *j* in the system, corresponding to any given species α and β, we employ a generalized Lennard-Jones (LJ) potential, $V_{\alpha\beta}(r_{ij}) = 4\epsilon\left[(\sigma/r_{ij})^{12} - A_{\alpha\beta}(\sigma/r_{ij})^{6}\right]$. Here, r_{ij} is the interatomic separation, σ is roughly the size of the repulsive hard core, and will be used as a characteristic length scale, and ϵ is the depth of the potential well, which will be adopted as the characteristic energy scale. To reduce the computational cost, the LJ potential is truncated at a distance $r_{ij} \cong 2.5\sigma$ [19]. The dimensionless *attraction* parameter $A_{\alpha\beta}$ modulates the attractive van der Waals interactions between the various atomic species in the system and, as a result, determines the wetting of the solid, as well as the interfacial tension between the immiscible liquids [15,20,21] . We consider two immiscible liquids, a high-wettability ($\alpha = \mathrm{H}$) and a low-wettability ($\alpha = \mathrm{L}$) one, with $A_{\mathrm{HL}} = 0.2$, corresponding to a surface tension $\gamma = 2.0\,\epsilon\,\sigma^{-2}$. We consider a single type of solid atoms composing both the walls as well as the nanoparticle ($\alpha = \mathrm{S}$). The low-wettability liquid interacts with the solid atoms with $A_{\mathrm{LS}} = 0.5$ and the interaction of the high-wettability liquid with the solid A_{HS} ranges from 0.5 to 0.9. This results in contact angles $\theta \leq 90°$, where θ is the contact angle of the liquid-liquid interface with the solid wall measured on the side of the high-wettability liquid, as indicated in Figure 1. The attraction parameter between atoms of the same species is always $A_{\alpha\alpha} = 1$. The number density of both liquids is $\rho_{\mathrm{L}} = 0.8\,\sigma^{-3}$, the wall density is $\rho_{\mathrm{W}} = 1.0\,\sigma^{-3}$ and that of the nanoparticle is $\rho_{\mathrm{P}} = 4.0\,\sigma^{-3}$. As in previous work, both walls and nanoparticle have a rigid fcc lattice structure [4]. It is important to note that since $\rho_{\mathrm{P}} > \rho_W$, the nanoparticle contact angle $\theta_p \leq \theta \leq 90°$ is smaller than that for the wall. In fact, the nanoparticle shows perfect wetting for $A_{\mathrm{HS}} \geq 0.8$, with the nanoparticle leaving the interface and staying inside the high-wettability liquid [19]. The temperature of the system is maintained at $\mathrm{T} = 1.0\,\epsilon/k_B$, where k_B is the Boltzmann constant, using a Nose-Hoover thermostat [8].

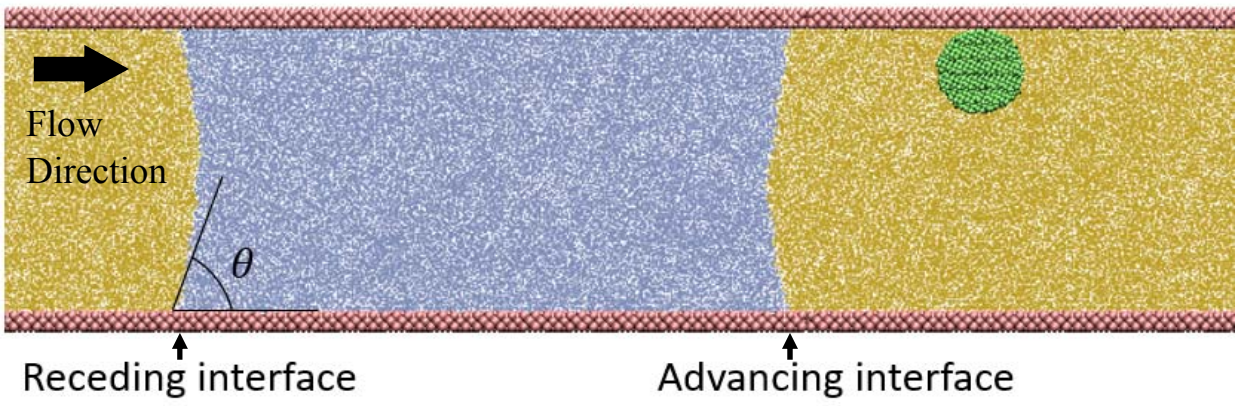

Figure 1: (Color online) Snapshot of two immiscible fluids moving past a nanoparticle deposited in a flat wall from a molecular simulation. The high-wettability liquid (H) is represented by the darker atoms and the lighter one corresponds to the low-wettability (L) liquid. The attraction parameters in the simulation are $A_{\mathrm{HS}} = 0.7$ ($A_{\mathrm{LS}} = 0.5$).

A snapshot from one of the MD simulations is presented in Figure 1, showing the two immiscible liquids confined between two parallel plates and moving past a nanoparticle deposited on one of the flat walls. The radius of the nanoparticle is $R = 6\sigma$, the separation between the two flat walls is $L_{\mathrm{y}} = 40\sigma$, the length of the channel along the forcing direction is $L_{\mathrm{x}} = 160\sigma$ and $L_{\mathrm{z}} = 20\sigma$. Periodic boundary conditions are applied in all three directions. We also indicate in the figure the *advancing* interface,

corresponding to the high-wettability liquid displacing the low-wettability one. Analogously, the *receding* interface displacement shown in Fig. 1 corresponds to the opposite case of a low-wettability liquid displacing a high-wettability one. Initially, we let the system equilibrate, starting with the particle in the low-wettability fluid, which results in its spontaneous adsorption onto the solid wall [15]. Then, a constant force f_x oriented along the channel is applied to each of the atoms on both liquids, which produces a total driving force F_{MD}. In what follows, we use non-dimensional units, based on the characteristic time $\tau = \sqrt{m\sigma^2/\epsilon}$, where m is the mass of the atoms, together with the characteristic length scale σ and energy scale ϵ of the modeled pairwise interactions between atoms.

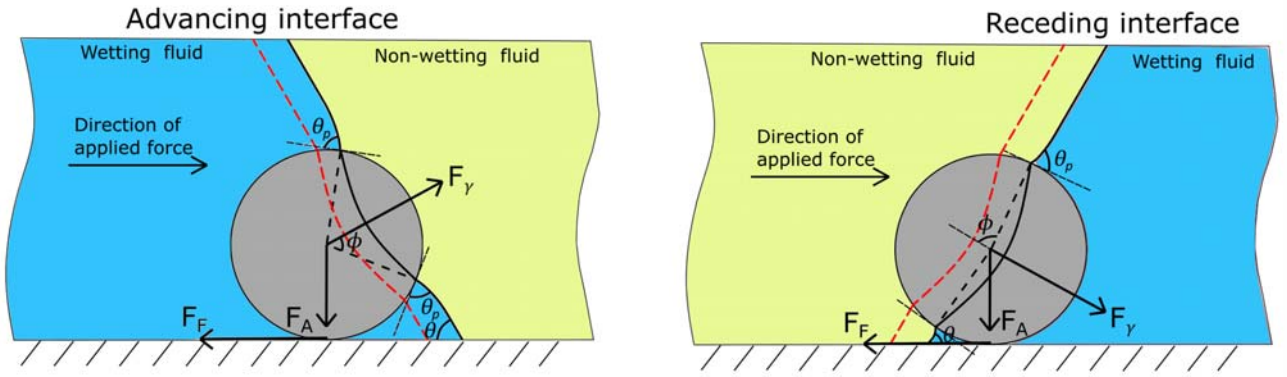

Figure 2: (Color online) Schematic of the force analysis on a spherical particle attached to a wall for an advancing interface (left; solid line) and a receding interface (right; solid line) with wall contact angle θ. The view corresponds to a cross-section of the system. Red dashed lines denote the interface equilibrium positions. At the liquid-liquid interface, the particle experiences surface tension forces (F_γ), in addition to the adhesion (F_A) and particle friction forces (F_F).

Figure 2 shows the schematic of the forces acting on a nanoparticle deposited on a solid substrate and interacting with an advancing (Fig. 2a) and a receding (Fig. 2b) interface. Three distinct type of forces act on the deposited particle and determine its behavior, possibly leading to mobilization and detachment. First, the adhesive and friction forces, F_A and F_F, which prevent normal detachment and horizontal sliding, respectively, originate from the particle-substrate interaction. In addition, when the liquid is moving, there would be a hydrodynamic-drag force, F_D, acting on the particle. Finally, capillary forces acting on the particle have two components, the surface tension force, F_γ, acting on the three-phase contact line as the liquid-liquid interface moves past the nanoparticle, and the capillary pressure force, F_{Pc}, originating on the Laplace pressure difference between the two liquids due to the (net) curvature of the liquid-liquid interface. The position of the contact line on the particle is determined by the filling angle ϕ, which for an advancing interface goes from 180° at initial contact with the high-wettability liquid to 0° when the particle is fully immersed in it. The filling angle goes from 0° to 180° as a receding interface moves past a particle. We note that the supplementary angle $\pi - \phi$ is sometimes used as the filling angle. The (red) dashed line in the figure indicates the equilibrium position $F_\gamma = 0$, which corresponds to $\phi = \theta_p$ and a flat interface in the absence of any geometric confinement. Therefore, when the filling angle is $\phi < \theta_p$ (or $\phi > \theta_p$), the surface tension force tends to increase (or decrease) the filling angle, as shown in Fig. 2. For a flat interface, the surface tension force is given by

$$F_\gamma = 2\pi R\gamma \sin\phi \sin(\theta_p - \phi), \quad (1)$$

which reaches its maximum value for $\phi = \theta_p/2$ (for $\phi < \theta_p$) or $\phi = (\theta_p + \pi)/2$ (for $\phi > \theta_p$) [23]. In the absence of confinement, there is no Laplace contribution to the capillary forces. On the other hand, in a channel of height H we can estimate the curvature (away from the particle) as $r_c = H/(2\cos\theta)$ and

the capillary pressure force can be estimated as $F_{P_c} = \pi R^2 sin^2\phi\, \Delta p = \pi R^2 sin^2\phi\gamma\, 2\cos\theta/H$, where we have used the Laplace equation $\Delta p = \gamma/r_c$ [7]. Comparing the two forces, we find that the capillary force is negligible in our system ($F_{Pc} \ll F_\gamma$) and should only be considered in highly confined situations where $H \cong R$ and $F_{Pc} \sim F_\gamma$. Therefore, in what follows we normalize all the forces in the system using the characteristic magnitude of surface tension forces, $|F_\gamma| \sim 2\pi R\gamma$; for example, the normalized surface tension force is $\tilde{F}_\gamma = F_\gamma/2\pi R\gamma$. Finally, ignoring the local curvature of the interface, and considering that both advancing and receding interfaces are driven in the same direction along the channel, the axial and normal components are obtained by projecting the force using the contact angle θ [24],

$$\left[\tilde{F}_\gamma^{\parallel} \quad \tilde{F}_\gamma^{\perp}\right] = \begin{cases} \sin^2\left(\frac{\theta_p}{2}\right)[\sin\theta \quad \cos\theta] & \text{if} \quad \phi < \theta_p \\ \cos^2\left(\frac{\theta_p}{2}\right)[\sin\theta \quad -\cos\theta] & \text{if} \quad \phi > \theta_p \end{cases}. \qquad (2)$$

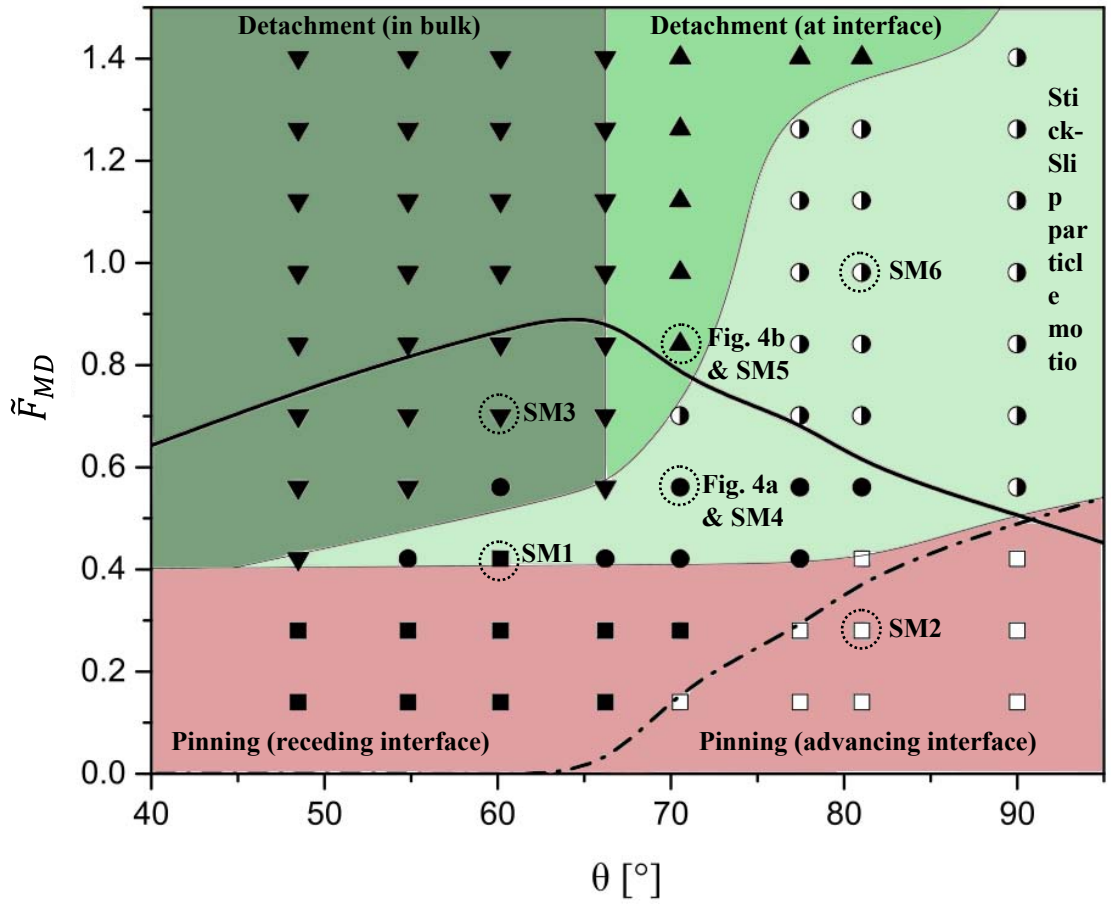

Figure 3: (color online) *Regime map* for the dynamics of a liquid-liquid interface moving past a deposited nanoparticle, parametrized by the normalized force driving the interface, $\tilde{F}_{MD}$, and the contact angle θ. The solid (dot-dashed) line corresponds to the maximum surface tension force in the horizontal direction as given in Eq. 2 for a receding (advancing) interface, $\phi > \theta_p$ ($\phi < \theta_p$). Symbols indicate simulations results. Square symbols indicate interface pinning of the receding (solid squares) or the advancing (open squares) interface. Circles indicate stick-slip motion of the particle along the wall due to its interaction with a receding interface (solid circles) or with both interfaces intermittently (open-solid circles). Solid triangles indicate desorption that occurs due to the interaction with the receding interface. The inverted triangles indicate that after adsorption the particles leave the interface and move into the high-wettability liquid. The shading indicates the regions where different behaviors are observed. The points with a dashed circle indicate that a movie of the simulation is available in the Supplemental Material [19].

Three distinguishable regimes were documented in our parametric study varying the driving force F_{MD} and contact angle θ: Interfacial *pinning* at small driving forces; *Stick-slip* and *Intermittent Stick-slip* particle motion at larger forces and high contact angles and *Rolling-induced detachment* at larger forces and small contact angles. These results are summarized in the *regime map* presented in Figure 3.

Interfacial Pinning. For small driving forces, we observe the pinning of the liquid-liquid interface when the surface tension force acting on the three-phase contact line can balance the external driving force ($F_\gamma^{\parallel} = F_{\mathrm{MD}}$). Therefore, the pinning regime only occurs for $\boldsymbol{\phi < \theta_p}$ for the advancing interface (dot-dashed line in Figure 3) and for $\boldsymbol{\phi > \theta_p}$ for the receding interface (solid line in Figure 3). We observe good agreement between this equilibrium prediction and simulation results, in that there is no pinning of the advancing interface for driving forces above the predicted critical values (indicated by the dot-dashed line in the figure), but we still observe pinning by the receding interface.

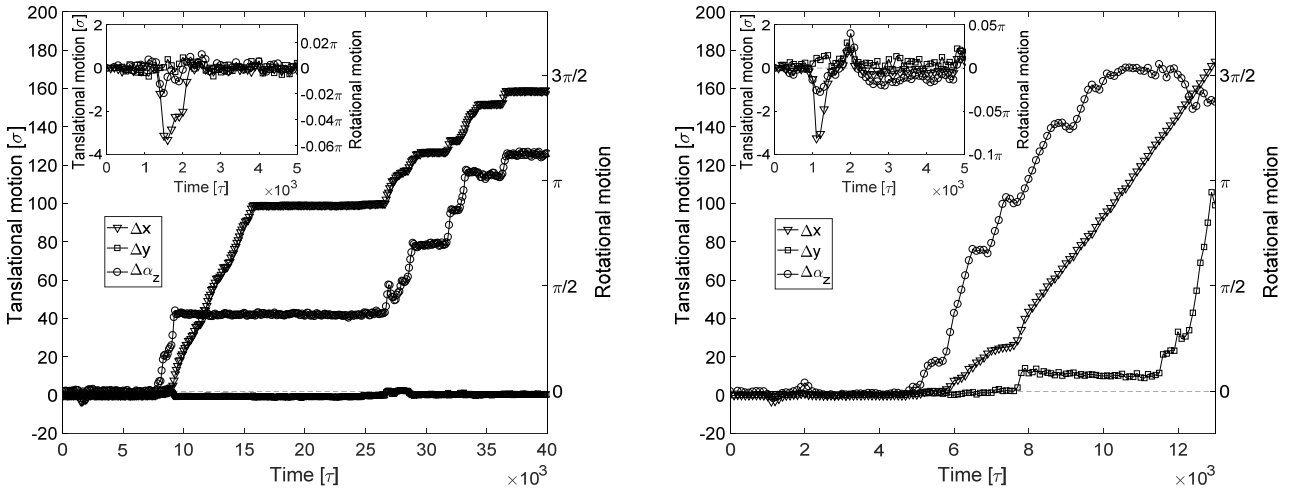

Figure 4: a) Stick-slip motion along the channel, vertical position, and incipient rotation (around the *z*-axis) for a nanoparticle at the receding interface. Inset shows the motion of the nanoparticle as it initially interacts with the receding interface. b) Rotation-induced nanoparticle dettachment by the receding interface. The plot shows $\Delta\alpha_z = \theta_p/2$, the rotation around the z-axis, the motion along the wall and the resulting separation normal to the wall (*y*-axis, amplified by a factor of 10 for clarity). Inset shows the initial interaction with the receding interface (Both cases are indicated in Figure 3.)

Stick-slip motion. At larger driving forces, we see that the liquid-liquid interface induces the sliding of the particle along the wall, even for forces below the solid line corresponding to the maximum surface tension force for the receding interface and independent of the contact angle. In this case, the surface tension force acting on the particle (intermittently) has to exceed the (maximum) friction force. To confirm that the surface tension force could overcome the friction force, we estimated the maximum friction force for a particle immersed in a single-phase liquid. We performed an independent set of simulations applying a force along the channel wall, $F_{\mathrm{ext}}^{\parallel}$, on a deposited particle. The minimum force leading to axial motion of the particle was $\tilde{F}_{\mathrm{ext}}^{\parallel} = \tilde{F}_F \approx 0.45$, with a small decrease as the attraction parameter between the liquid and the wall increases. Although these measurements are performed in a single-phase fluid, the sliding behavior in the presence of the liquid-liquid interface is observed at values of the driving force similar to the single-phase friction force, $\tilde{F}_{\mathrm{MD}} \gtrsim 0.4$. Interestingly, the motion is not a continuous sliding but rather analogous to the stick-slip motion previously observed in single-phase fluids (see Figure 4a) [15]. Note that the particle remains at the liquid-liquid interface during the stick-slip motion, resulting in a pinning-sliding intermittent motion of the interface itself. We also examined

the detailed dynamics of the nanoparticle and observed that rotation of the nanoparticle along the z-axis precedes the sliding motion, but no continuous rotation is observed as the particle moves with the interface, as shown in Figure 4a.

Intermittent Stick-Slip motion. Another regime change is observed for larger external forces, above the maximum of the static surface tension force for the receding interface given in Eq. 2. In this case, a different type of intermittent motion is observed (indicated by the half-solid half-empty symbols in Figure 3), the particle is alternatively carried by the advancing and receding interfaces. It is also important to note a *reverse motion* that occurs as the receding interface makes contact with the particle. During this transient, when $\boldsymbol{\phi < \theta_p}$ the surface tension force pulls the particle upstream in the horizontal direction and away from the wall. This is also shown in Figure 4a where we observe a (small) upstream translation along the wall. However, no significant displacement is observed in the normal direction. We note that, the presence and magnitude of partial hydrodynamic slip at the solid-liquid interfaces, which also depends the solid-liquid attraction parameter [25], was not explored in this work, but could also affect the emergence of stick-slip motion and even detachment, and is worth investigating.

Rolling-induced detachment. For large driving forces, $\tilde{F}_{MD} \gtrsim 1$, we observe some cases of nanoparticle detachment induced by the receding interface. Interestingly, in this case the equilibrium calculations presented in Eq. (1) show that the receding interface exerts a negative normal force ($\boldsymbol{\phi > \theta_p}$). On the other hand, the external forcing in this case is comparable to the Laplace pressure for a curvature similar to the width of the channel, and the deformation of the interface cannot be neglected. In fact, we have observed the formation of drops of the low-wettability liquid immersed in the high-wettability liquid for forces $\tilde{F}_{MD} \approx 1$. As a result, the local orientation of the liquid-liquid interface can no longer be approximated by the contact angle with the wall, as assumed in Eq. (1). To estimate the required detachment force, we measured the force normal to the substrate that is required to pull the particle off the surface of the solid (*pull-off force*) and obtained $\tilde{F}_{\mathrm{A}}^{\max}$ increasing from 2 to 4 as the attraction parameter increases. Interestingly, this value is larger than $\widetilde{F_\gamma}$, independent of its orientation. In addition, and similar to the sliding case, we observe that detachment is always preceded by rotation of the nanoparticle along the z-axis. Figure 4b shows both the rotation of the nanoparticle, together with its motion along the wall as well as its separation from the initial position normal to the wall. These results indicate that there is significant rotation preceding (and probably leading to) any separation from the wall, which renders the static calculations no longer valid and demonstrates the importance of interfacial dynamics in particle detachment. Detachment is commonly observed at intermediate contact angles, when there is significant contrast in the wetting behavior of the two liquids, and it occurs as the high-wettability liquid surrounding the particle is displaced by the low-wettability liquid. After detachment, the contact angle determines whether the particle remains at the interface ($\theta_p > 0°$) or not ($\theta_p = 0°$), as indicated by the up- and down-pointing triangles, respectively, in Figure 3.

The results in this work document the key role of dynamic effects in the mobilization of adsorbed nanoparticles by the forced displacement of a liquid-liquid interface and indicate that particle detachment could be significantly underestimated by static models. For sufficiently small values of the driving force, the nanoparticles simply pin the liquid-liquid interface and the observed behavior can be predicted by a static force balance. Above the critical force magnitude predicted by a static analysis, the nanoparticles undergo stick-slip motion with incipient rotation inducing the transition from stick to sliding motion. Rotation also plays a crucial role for larger forces, in this case the interaction of the particle with the receding interface results in particle detachment at moderate contact angles. Dynamic effects associated with particle rotation and the observed stick-slip and sliding motion can result in the

remobilization and removal of nanoparticles for driving forces that are much smaller than the critical value predicted by conventional static models. Hence, static force balances can significantly overestimate the forces required for particle detachment and underestimate the corresponding remobilization rates employed in continuum models such as colloid filtration theory. Considering the dynamic effects and different regimes documented in this work it is possible to develop improved transport models to better predict the fate of colloidal particles in multiphase flows under different wetting conditions and for physical dimensions ranging from nano- to microscales. Experiments to verify the main findings of this work are being pursued and preliminary results for microparticles interacting with a moving oil-aqueous interface are presented in the supplementary material [19]. T.Y and G.D were partially supported by the National Science Foundation Grant No. 1437478. D. S. and J. F. were partially supported by the National Science Foundation Grant No. 1436482. This work used the Extreme Science and Engineering Discovery Environment (XSEDE), which is supported by National Science Foundation grant number ACI-1548562.

[1] J. F. McCarthy and L. D. McKay, Vadose Zone J. **3**, 326 (2004).
[2] B. V. D. Bruggen, C. Vandecasteele, T. V. Gestel, W. Doyen, and R. Leysen, Environ. Prog. **22**, 46 (n.d.).
[3] J. Ochi and J.-F. Vernoux, J. Hydrol. **208**, 237 (1998).
[4] N. Tufenkji and M. Elimelech, Langmuir **21**, 841 (2005).
[5] I. L. Molnar, W. P. Johnson, J. I. Gerhard, C. S. Willson, and D. M. O'Carroll, Water Resour. Res. **51**, 6804 (2015).
[6] E. Goldberg, M. Scheringer, T. D. Bucheli, and K. Hungerbühler, Environ. Sci. Technol. **48**, 12732 (2014).
[7] M. Flury and S. Aramrak, Water Resour. Res. **53**, 5247 (2017).
[8] S. A. Bradford and S. Torkzaban, Vadose Zone J. **7**, 667 (2008).
[9] A. Fogden, M. Kumar, N. R. Morrow, and J. S. Buckley, Energy Fuels **25**, 1605 (2011).
[10] J. Bergendahl and D. Grasso, Chem. Eng. Sci. **55**, 1523 (2000).
[11] J. J. Lenhart and J. E. Saiers, Environ. Sci. Technol. **36**, 769 (2002).
[12] S. Aramrak, M. Flury, J. B. Harsh, and R. L. Zollars, Environ. Sci. Technol. **48**, 7272 (2014).
[13] Q. Zhang, S. M. Hassanizadeh, N. K. Karadimitriou, A. Raoof, B. Liu, P. J. Kleingeld, and A. Imhof, Water Resour. Res. **49**, 8005 (2013).
[14] Q. Zhang and S. M. Hassanizadeh, Chem. Eng. Sci. **168**, 437 (2017).
[15] G. Drazer, J. Koplik, A. Acrivos, and B. Khusid, Phys. Rev. Lett. **8924**, 4501 (2002).
[16] G. Drazer, B. Khusid, J. Koplik, and A. Acrivos, Phys. Fluids **17**, 17102 (2005).
[17] G. Drazer, B. Khusid, J. Koplik, and A. Acrivos, Phys. Rev. Lett. **95**, 016102 (2005).
[18] S. Plimpton, J. Comput. Phys. **117**, 1 (1995).
[19] See Supplemental Material at [URL Will Be Inserted by Publisher] for Simulation Details and Movies., n.d.
[20] C. E. Colosqui, T. Teng, and A. Rahmani, Phys. Rev. Lett. **115**, 154504 (20158).
[21] S. Razavi, I. Kretzschmar, J. Koplik, and C. E. Colosqui, J. Chem. Phys. **140**, 1 (2014).
[22] M. P. Allen and D. J. Tildesley, *Computer Simulation of Liquids* (Clarendon Press, 1999).
[23] V. Lazouskaya, L.-P. Wang, D. Or, G. Wang, J. L. Caplan, and Y. Jin, J. Colloid Interface Sci. **406**, 44 (2013).
[24] A. F. M. Leenaars and S. B. G. O'brien, Philips J Res **44**, 183 (1989).
[25] N. V. Priezjev, Phys. Rev. E **75**, (2007).